Applied Scientific Research **54:** 163–176, 1995.

Turbulent Breaking of Overturning Gravity Waves below a Critical Level

ANDREAS DÖRNBRACK, THOMAS GERZ and ULRICH SCHUMANN
DLR, Institute of Atmospheric Physics, D-82230 Oberpfaffenhofen, Germany

Received 11 July 1994; accepted in revised form 19 February 1995

Abstract. The interaction of an internal gravity wave with its evolving critical layer and the subsequent generation of turbulence by overturning waves are studied by three-dimensional numerical simulations. The simulation describes the flow of a stably stratified Boussinesq fluid between a bottom wavy surface and a top flat surface, both without friction and adiabatic. The amplitude of the surface wave amounts to about 0.03 of the layer depth. The horizontal flow velocity is negative near the lower surface, positive near the top surface with uniform shear and zero mean value. The bulk Richardson number is one. The flow over the wavy surface induces a standing gravity wave causing a critical layer at mid altitude. After a successful comparison of a two-dimensional version of the model with experimental observations (Thorpe [21]), results obtained with two different models of viscosity are discussed: a direct numerical simulation (DNS) with constant viscosity and a large-eddy simulation (LES) where the subgrid scales are modelled by a stability-dependent first-order closure. Both simulations are similar in the build-up of a primary overturning roll and show the expected early stage of the interaction between wave and critical level. Afterwards, the flows become nonlinear and evolve differently in both cases: the flow structure in the DNS consists of coherent smaller-scale secondary rolls with increasing vertical depth. On the other hand, in the LES the convectively unstable primary roll collapses into three-dimensional turbulence. The results show that convectively overturning regions are always formed but the details of breaking and the resulting structure of the mixed layer depend on the effective Reynolds number of the flow. With sufficient viscous damping, three-dimensional turbulent convective instabilities are more easily suppressed than two-dimensional laminar overturning.

Key words: stably stratified shear flow, critical level formation, wave-turbulence transition

1. Introduction

The generation of turbulence by overturning internal gravity waves is an important factor in the microscale dynamics of atmosphere and ocean. For instance, the mechanism is thought to be the primary cause for clear-air turbulence [15] and for the occurrence of thin turbulent layers in the free atmosphere [12, 16, 18]. Some theories and numerical attempts exist to explain how overturning waves are excited, however, it is not known how these waves break in detail. As possible instability mechanisms Kelvin–Helmholtz and convective instabilities are discussed. Another fundamental mechanism that leads to the breaking of gravity waves is the interaction of an internal gravity wave with its critical level. This is the subject of our study.

In a shear flow, the critical level is the height where the phase speed of a wave equals the mean flow speed [2]. The wave propagation is strongly modified due to the formation of a critical layer: waves above the critical level decay (the trapping effect of the critical layer) and the wave transfers momentum from below upwards into the mean motion beneath the critical level. Depending on the excitation energy of the initial wave field, shear, and stratification of the basic flow, turbulence can be generated transferring kinetic energy to smaller scales.

The gravity-wave critical-layer interaction is difficult to study observationally in the free atmosphere because of the broad spectrum of scales which prevents the observation of isolated events. In the planetary boundary layer some attempts have been made to demonstrate the critical layer effect [11, 14]. In the laboratory, the interaction has been observed under controlled conditions by defining one wavelength and prescribing a mean velocity profile. So far, only a few (mostly qualitative) observations are known [3, 7, 21].

Thorpe [21] used a simple experiment device: a long rectangular tube, filled with salt-stratified water. The lower boundary had sinusoidal corrugations which excited internal gravity waves with zero phase speed in the stratified shear flow. The shear flow with zero mean was forced by tilting the tube horizontally by a small angle. Its strength depends on this angle and the time of tilting. As in other experiments, no wavy motion could be observed above the critical layer. The vertical propagation of the internal gravity waves was stopped near the critical layer and regions of reduced density gradients developed over the troughs of the surface waves. These regions became gravitationally unstable (Kelvin–Helmholtz instability was not observed). As a test we repeat Thorpe's experiment numerically. Although Thorpe's experiment dealt with salt-stratified water we interpret it in terms of a thermally stratified medium, because we are ultimately interested in atmospheric flows.

As the main aim of this paper, we present results of two three-dimensional numerical simulations of the interaction of a vertically propagating gravity wave with its critical layer. The simulations differ in the treatment of viscosity in the flow. We use a direct numerical simulation (DNS) with constant viscosity and a large-eddy simulation (LES) where the subgrid scales are modelled by a stability-dependent first-order closure. Hence, the former case simulates a flow at rather moderate Reynolds number, whereas in the latter case the molecular viscosity is zero and subgrid scale turbulent mixing is limited to local regions with strong velocity deformation and low Richardson numbers. Two different regimes can be identified. A laminar breaking apears in the case of DNS where the continuous rolling-up of density surfaces resembles the mixing. In the LES the breakdown of the convectively unstable regions occurs immediately after the appearance of instability and small-scale turbulent motion is generated.

Section 2 introduces the numerical model. The comparison with the experimental results of Thorpe [21] is presented in Section 3. Section 4 discusses the results of the three-dimensional simulations.

2. Numerical Model

We consider a thermally stably stratified fluid with the temperature $\vartheta = \vartheta_0 + \Theta + \theta$. The background temperature ϑ_0 is constant, the stratification is characterized by the mean part Θ whereas the fluctuations are denoted by θ. The mean part is defined by the initial background Brunt–Väisälä frequency N as

$$N^2 = \frac{g}{\vartheta_0} \frac{\mathrm{d}\Theta}{\mathrm{d}z} . \tag{1}$$

We define the reference values for lenght, velocity, temperature, and density, as H, ΔU, $\Delta\Theta$, and ρ_0, respectively, where ΔU and $\Delta\Theta$ are the velocity and temperature differences across the vertical depth H and ρ_0 is the reference density in the model which uses the Boussinesq approximation. The bulk Richardson number is defined by

$$\mathrm{Ri}_B = \frac{N^2}{\bar{S}^2} = \frac{g\Delta\Theta H}{\vartheta_0 \Delta U^2} , \tag{2}$$

where $\bar{S} = \Delta U/H$ is the mean shear. The conservation laws for mass, momentum and integral energy in curvilinear coordinates read

$$\frac{\partial}{\partial \bar{x}^d}(\rho_0 V G^{dq} u q) = 0, \tag{3}$$

$$\begin{aligned} &\frac{\partial}{\partial t}(V u_i) + \frac{\partial}{\partial \bar{x}^d}(V G^{dq} u_q u_i) \\ &\quad = -\frac{1}{\rho_0}\frac{\partial}{\partial \bar{x}^g}(V G^{gi} p) - \frac{\partial}{\partial \bar{x}^d}(G^{ds}(V F_{is})) + V\frac{\theta}{\vartheta_0}\delta_{3i} , \end{aligned} \tag{4}$$

$$\frac{\partial}{\partial t}(V\theta) + \frac{\partial}{\partial \bar{x}^d}(V G^{dq} u_q \theta) + V u_3 \frac{\mathrm{d}\Theta}{\mathrm{d}x_3} = -\frac{\partial}{\partial \bar{x}^d}(G^{dr}(V Q_r)). \tag{5}$$

The Cartesian velocity components $u_i = (u, v, w)$ and the temperature perturbation θ are computed on a terrain following coordinate system in which the curvilinear coordinates $(\bar{x}, \bar{y}, \bar{z})$ are related to Cartesian coordinates (x, y, z) according to

$$\bar{x} = x, \quad \bar{y} = y \quad \text{and} \quad \bar{z} = \eta(x, z) = H\frac{(z - h)}{(H - h)} . \tag{6}$$

The Jacobian of the transformation $G^{ij} = \partial \bar{x}_i / \partial x_j$ is $V = (\det G^{ij})^{-1}$ and $h(x)$ is the prescribed height of the bottom surface. Details of the implementation of this coordinate transformation in the numerical code and its solution procedures are described in Krettenauer and Schumann [9]. The diffusive fluxes are

$$V F_{ij} = -K_M V 2 D_{ij}, \quad V Q_i = -K_H \frac{\partial}{\partial \bar{x}^r}(V G^{ri}\theta). \tag{7}$$

In the case of the DNS, $K_M = 1/\mathrm{Re}$ and $K_H = 1/\mathrm{RePr}$ with $\mathrm{Re} = \Delta U H/\nu$ and $\mathrm{Pr} = \nu/\gamma$, where ν and γ denote the kinematic viscosity and thermal conductivity. In the case of the LES, $K_M = \nu_{\mathrm{turb}}$ and $K_H = \nu_{\mathrm{turb}}/\mathrm{Pr}_{\mathrm{turb}}$. The turbulent viscosity is determined as a function of the local Richardson number as suggested by Lilly [10]:

$$\nu_{\mathrm{turb}} = \begin{cases} \Lambda^2 |S - \bar{S}| \sqrt{1 - \dfrac{\mathrm{Ri}}{\mathrm{Ri}_c}}, & \text{when} \quad \mathrm{Ri} < \mathrm{Ri}_c = 1 \\ 0 & \text{otherwise,} \end{cases} \tag{8}$$

where S is the second invariant of the deformation tensor in terrain following coordinates

$$S = \sqrt{2 D_{ij} D_{ij}}, \quad D_{ij} = \frac{1}{2} \frac{1}{V} \frac{\partial}{\partial \bar{x}^r} (V G^{rj} u_i + V G^{ri} u_j). \tag{9}$$

The mean shear $\bar{S}$ is subtracted from the local deformation S in Eq. 8 so that the turbulent diffusivity is zero in the unperturbed mean flow and essentially nonzero only in the perturbated regions where $\mathrm{Ri} < 1$. The mixing scale Λ is related to the grid spacings as $\Lambda = 0.1(\Delta x + \Delta y + \Delta z)/3$. The turbulent Prandtl number is set to a constant value.

The computational domain covers one wavelength λ of the surface undulation with amplitude δ, i.e., $h(x) = \delta \cos(2\pi x/\lambda)$. Cyclic boundary conditions are used in the streamwise (x) direction and in the cross-stream (y) direction. Since we are not interested in resolving the viscous surface layers of the laboratory model, the boundary conditions

$$\frac{\partial \theta}{\partial z} = 0, \quad \frac{\partial u}{\partial z} = \frac{\Delta U}{H}, \quad \frac{\partial v}{\partial z} = 0, \quad \frac{\partial (V F_{13})}{\partial z} = 0 \tag{10}$$

are used at the upper and lower surfaces. The normal velocity is zero at the wall boundaries. Hitherto, the numerical code has been applied to the simulation of flow over wavy boundaries under convective and neutral conditions and details of the numerical method are described in e.g. [4, 9, 13, 17].

3. Comparison with Measurements for a Weakly Nonlinear Shear Flow

In this section, we compare the results of a two-dimensional DNS with the measurements of Thorpe [21] who observed the internal gravity-wave critical-layer interaction in the laboratory. In the experiment, the mean velocity was zero and a uniform shear was induced initially by tilting the tube by the angle α relative to the horizontal for a time t_α. The evolving shear flow, which depends on α, t_α and N according to $\Delta U/H = N^2 t_\alpha \sin\alpha$ [20], was weakly nonlinear. The lower undulated surface, consisting of sixteen sinusoidal waves, excited the internal gravity waves with zero phase speed in the shear flow. The experiments in the salt-stratified

water took place at $\mathrm{Re} = \Delta U H/\nu \approx 50000$ and at a Schmidt number of about 500.

In the simulation, we replace the sixteen floor waves by a single one and cyclic boundary conditions. In accordance with the experiment, we use $\lambda = 1.5625H$, $\delta = 0.03125H$, $\alpha = 7.1°$, and $t_\alpha = 3.75$ s. The initial velocity distribution and the mean temperature field are given by

$$U(z) = \frac{\Delta U}{H}(z - 0.5H), \quad \frac{\Theta(z)}{\vartheta_0} = \frac{\Delta\Theta}{\vartheta_0}\frac{(z - 0.05H)}{H}, \tag{11}$$

where $\Delta\Theta/\vartheta_0 = N^2H/g$. With $N = 2.06\ \mathrm{s}^{-1}$ and $H = 0.16$ m from the laboratory experiment, the bulk Richardson number is $\mathrm{Ri}_B \approx 1.1$. Initial velocity and temperature fluctuations are set to zero. We resolve the domain by 200×128 meshes and achieve the same Reynolds number as in the experiment. We cannot achieve Schmidt numbers of 500 numerically due to limited computer capacity. However, the value of Schmidt number is of minor importance in this context since the flow is only weakly nonlinear [21]. Thus, dynamics at small scales, where the correct treatment of Schmidt number becomes important, are negligible. Therefore, we consider the effect of stratification in terms of heat instead of salt and set the Prandtl number $\mathrm{Pr} = 1$.

In Fig. 1, we compare our results with the observations of Thorpe [21] when the tube is returned into the horizontal position and the shear flow is no longer accelerated. In the observations, layers of constant density were marked by adding dye. These layers have a certain thickness depending on the experimental set-up. The deformation of these black and white regions illustrates the wave propagation with time. For a quantitative comparison with the measurements, we plot the contour lines of the temperature field with a constant increment $\Delta\vartheta = 0.0032\Delta\Theta$ in such a way that the thickness and the position of the areas between adjacent contour lines correspond to the black and white layers documented in the photographs of the observations. In addition, the most interesting areas in the middle of the numerical domain are emphasized as in the laboratory experiment.

At the beginning, the lines of constant temperature, i.e. colder (heavier) fluid is lying in the trough and the fluid gets warmer (lighter) with increasing height. The mean flow is towards the left near the surface and towards the right at the top boundary. The overall features of the flow evoluton in the laboratory and in the numerical simulation are obviously similar. The sinusoidal corrugations at the bottom surface excite internal gravity waves that propagate vertically towards the critical level (Fig. 1a). The amplitude of the waves increases with height but falls to zero at the critical level. No wavy motion is found above this level which acts as an absorber whereby momentum is transfered to the mean flow causing an advection in the positive x-direction. Regions of reduced vertical temperature (density) gradients (characterized by thickening of the marked layers) are mainly found above the trough of the undulating surface (Fig. 1b). Because of the reduced gradients, the local Richardson number drops and these regions become convectively (grav-

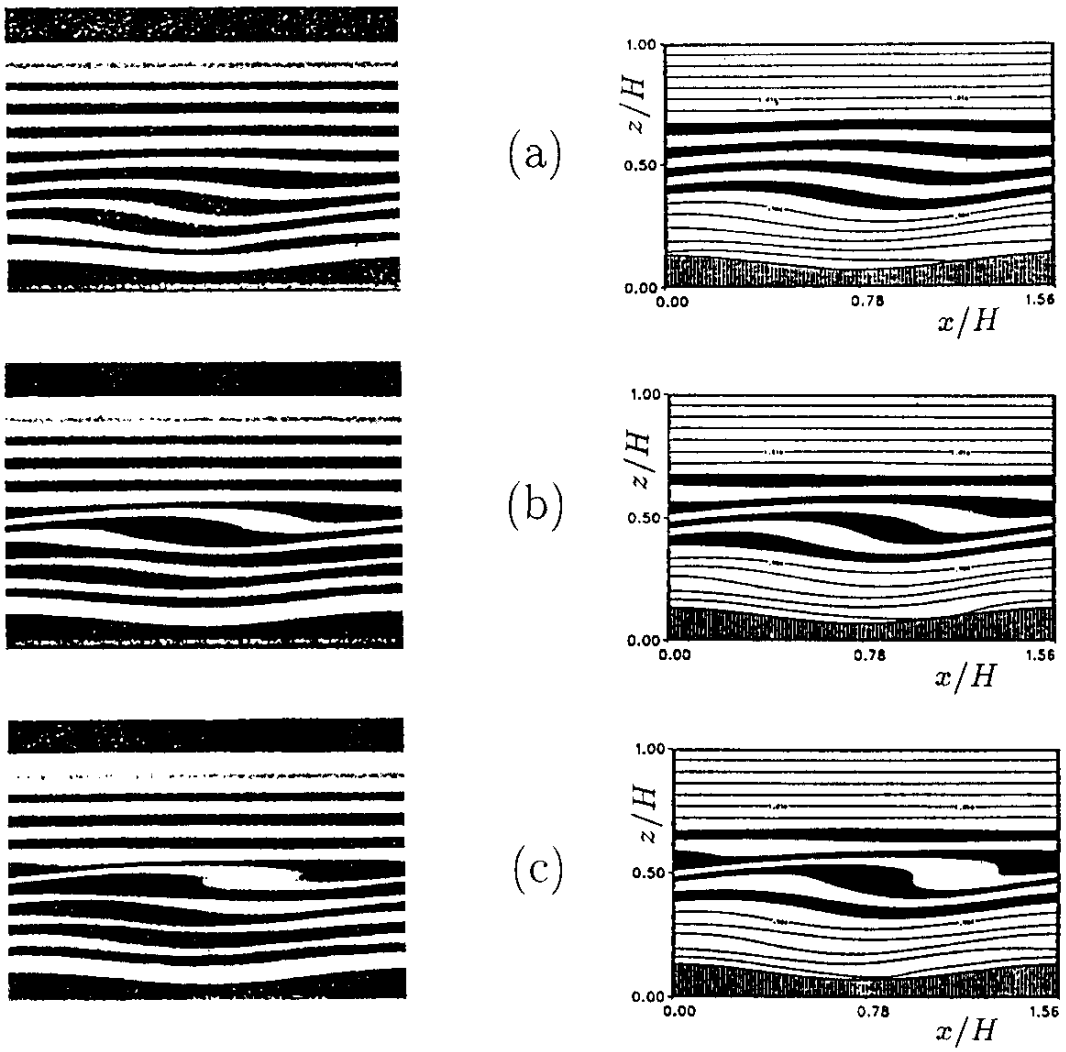

Fig. 1. Comparison with the observations of Thorpe [21, Fig. 4e, h, j]. Left side: experimental results at $t = 4.5$ s (a), $t = 7.9$ s (b), and $t = 10.2$ s (c). Right side: results of the numerical simulation at corresponding time.

itationally) unstable, where the advection puts colder (heavier) fluid over warmer (lighter) fluid (Fig. 1c), which finally leads to the wave breaking. Between these sites of instability the vertical gradient is enhanced and the black and white areas over the crest of the undulating surface become thinner, a structure similar to that found for Kelvin–Helmholtz instability.

Although we have not used the same boundary conditions as in the experiment (no friction), excellent agreements with the observed flow patterns was obtained. Obviously, the viscous friction at the top and bottom surface is of minor importance in this case. The viscous boundary layer thickness at a flat wall grows as $(\nu t)^{1/2}$, i.e. stays below the small value of $0.02H$ for $t < 10.2$ s. A slight difference can be seen between the observed and the computed position of the unstable region.

In the computations, overturning occurs further to the right and a more unstable region is visible also on the left side. This may be caused by differences in the shear profile because we do not simulate the detailed transition from the tilted to the nontilted tube position. Further tests have shown that the acceleration of the mean flow below the critical level depends very much on the Reynolds number. The lower the Reynolds nuumber the weaker is the transfer of momentum to the mean flow and the smaller the advection causing the breaking.

To conclude we find that our numerical method provides a good reproduction of Thorpe's experiment of the formation of a critical level and the onset of overturning gravity waves in a weakly nonlinear shear flow. Hence, the method is suited for this kind of studies.

4. Breaking of Internal Gravity Waves

Encouraged by the good performance of the numerical method as shown by the test presented in the former section (and comparisons to linear solutions), we now study the turbulent breakup of overturning gravity waves below the critical layer by means of three-dimensional DNS and LES.

4.1. Experimental set-up

We solve the governing equations 3 to 5 for a three-dimensional incompressible Boussinesq fluid in a computational domain as in the test case before but with a lateral domain siez of $0.3125H$. The characteristic length scale of the expected three-dimensional structures caused by the breaking is of the order of the thickness of the resulting mixed layer. This scale is essentially less than a quarter of H. Thus, the domain is large enough to capture all scales. The finite difference grid is uniform in all space directions of the transformed coordinates using $150 \times 30 \times 96$ nodes. The time step is $\Delta t = 0.005H/\Delta U$ and both simulations run until $t = 40H/\Delta U$ which is equal to $20/\pi$ buyonacy periods.

At time $t = 0$, the fluid is characterized by Eq. 11 for both cases. The mean flow with constant shear $\bar{S}$ is towards the left in the lower half and towards the right in the upper half of the domain such that the fluid speed is zero at $z = 0.5H$. The sinusoidal surface excites gravity waves with zero phase speed. Hence, the critical layer is situated at $z = 0.5H$. The bulk Richardson number Ri_B is one. The ratio of the horizontal wavenumber to the Scorer parameter $2\pi|U(z)|/\lambda N$ is approximately 2 near the bottom and decays with increasing height due to the linear velocity profile. According to the linear theory of wave motion (e.g. [19]), internal gravity waves are possible if the ratio is less than 1, i.e. in our specific case for heights $z > 0.2H$. The velocity fluctuations are set to zero, but the temperature field is randomly disturbed initially by random fluctuations with a volume-averaged variance $\sqrt{\overline{\theta^2}} = 0.001$. Some three-dimensional disturbances are necessary because otherwise the flow would remain in a two-dimensional state

for all times. It does not matter whether the disturbances are introduced in the velocity field or in terms of local buyoancy disturbances.

In the case of DNS, we set $K_M = 1/\mathrm{Re} = 1/50000$ and $\mathrm{Pr} = 1$ in Eq. 7. For the LES, the eddy viscosities $K_M = K_H$ are calculated by means of Eq. 8 with $\mathrm{Pr}_{\mathrm{turb}} = 1$ [8]. Hence, both cases differ only in the subgrid scale model representing different effective Reynolds numbers.

4.2. Results and discussion

For both simulations we produced sequences of picturse showing temperature contours of the evolving flow. From these sequences we learn that the temporal development of the wave structure up to the time $t \approx 20H/\Delta U$ is similar in both cases and essentially analogous to the two-dimensional results shown in Fig. 1: the flow over the wave surface excites internal gravity waves which propagate upward and generate regions of reduced (enhanced) stability over the trough (crest) of the corrugated surface. Above the critical level, no or very small wave motion is observed. Any initial wave disturbance above that level is damped. Below the critical level, in the early state, the main effect is the long lasting acceleration of the mean flow in the positive x-direction. This acceleration is opposite to the direction of $U(z)$ for $z < 0.5H$ (see Fig. 4 below). The disturbed mean flow raises heavier fluid over lighter one directly beneath the critical level, whereas the mean advection in the negative x-direction at lower altitudes moves lighter fluid under heavier one. Between these levels, the fluid stagnates and a convectively unstable region is formed. This process creates the primary roll which extends over almost one wavelength λ and has a thickness of $\approx 0.1H$. At the surface, we see isothermals reflecting the cold fluid, that was initially resting in the troughs, advected in the negative x-direction with time.

After $t \approx 20H/\Delta U$, the flow starts to evolve differently for DNS and LES. Figure 2 shows contour lines of the instantaneous temperature fields ϑ/ϑ_0 at $t = 24H/\Delta U$ in a x–z-cross-section in the center plane. In the case with uniform viscosity, a large region of warmer fluid is advected towards the left under colder fluid in the middle of the domain below the critical level without any drastic mixing. On the other hand, in the LES, small parcels from the region of colder (warmer) fluid have left their origin and sink down (rise up): this is the onset of the *turbulent* break-up of the overturning gravity waves. Note that the position and vertical extension of the breaking area are almost the same in both cases. The DNS and LES results differ in the inner structure and the degree of chaos of these mixing layers (see Fig. 3).

In the DNS, the onset of smaller-scale three-dimensional instabilities is damped by viscous friction. The flow is essentially laminar and the main characteristic of the breaking is the continuous generation of coherent secondary rolls induced by shear and the primary roll. This triggers small-scale gravity waves which grow in amplitude and overturn themselves (Fig. 3a). The secondary rolls have a typical

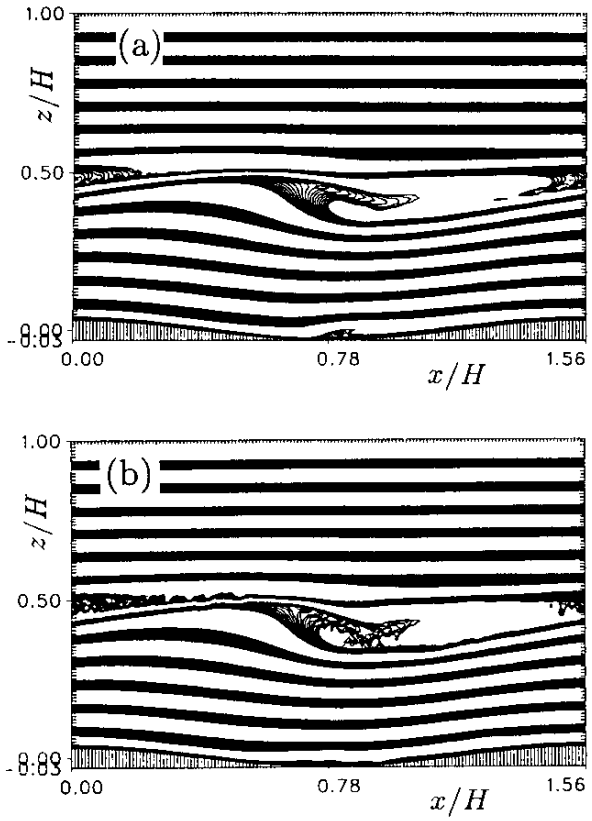

Fig. 2. Contour lines of ϑ/ϑ_0 at $t = 24H/\Delta U$ for the DNS (a) and the LES (b).

length of about $\lambda/3$ and they are advected in the negative x-direcction by the mean flow. Due to the entrainment of fluid from lower altitudes, the mixing layer widens downwards and covers a vertical depth of $\approx H/4$ at $t = 40H/\Delta U$.

In the LES, the fluid is less viscous and an overturning wave collapses into three-dimensional turbulence quickly when the flow becomes convectively unstable. Between $t = 30$ and $t = 36H/\Delta U$ there is also a tendency to build up a secondary roll structure but this is destroyed quickly by the mixing. At the end of the simulation we find large areas of reduced vertical density gradients; the flow in the breaking region is well mixed and only small portions of the fluid are still convectively unstable (Fig. 3b).

Now, we turn to flow statistics. Figure 4 shows the mean profile (averaged on planes $\eta = \text{const}$) of the u-velocity and of the local Richardson number, which is defined as

$$\mathrm{Ri} = \frac{g}{\vartheta_0} \frac{\partial\vartheta/\partial z}{(\partial u/\partial z)^2 + (\partial v/\partial z)^2}, \tag{12}$$

at five instants of time for the DNS. The LES profiles are similar, therefore we only discuss the results for the DNS. Below the critical level $\eta = 0.5H$, the mean velocity increases in time; the final maximum speed-up at $t = 40H/\Delta U$ is

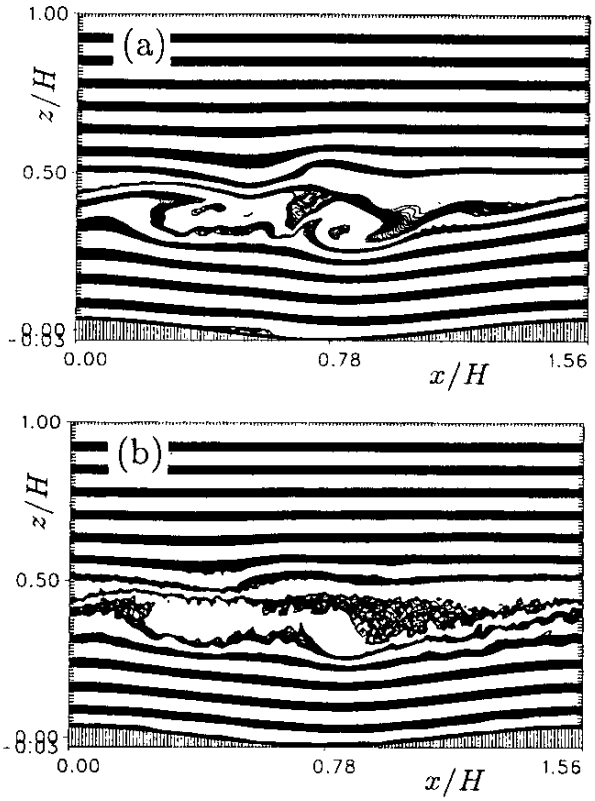

Fig. 3. Contour lines of ϑ/ϑ_0 at $t = 40H/\Delta U$ for the DNS (a) and the LES (b).

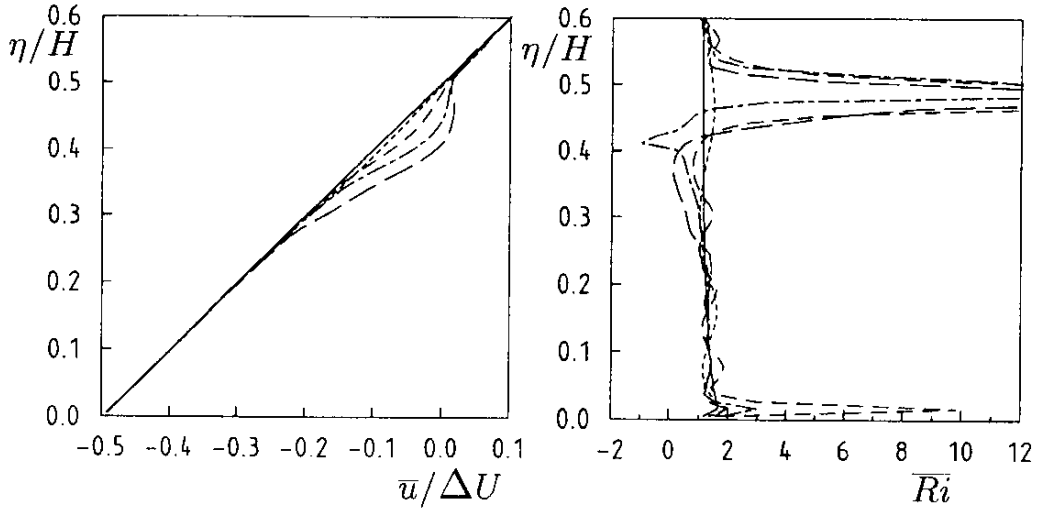

Fig. 4. Mean profiles of the horizontal velocity and the Richardson number at five different times for the DNS. The profiles are obtained by averaging over planes $\eta = \text{const}$. The times are $t = 0$ ——, $t = 6H/\Delta U$ - - - - -, $t = 12H/\Delta U$ – – –, $t = 24H/\Delta U$ – · – · –, $t = 40H/\Delta U$ — — —.

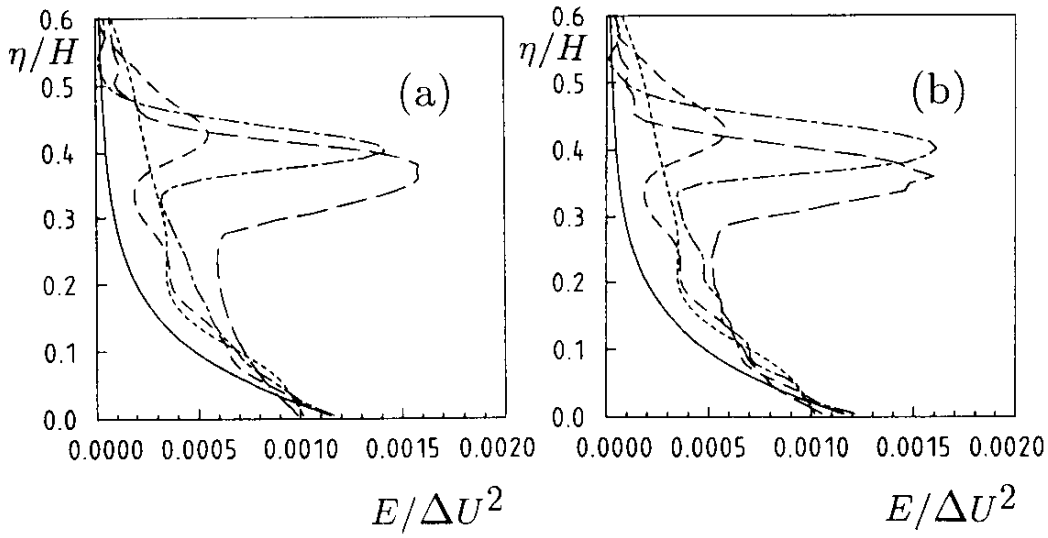

Fig. 5. Profiles of the kinetic energy $E = 0.5(\overline{u'^2} + \overline{v'^2} + \overline{w'^2})$ for the DNS (a) and the LES (b). Line coding and averaging as in Fig. 4.

$0.089\Delta U$ in the DNS and $0.092\Delta U$ in the LES. The layer directly influenced by the momentum transfer between the wave and the mean flow has a thickness of about $H/4$. We expect that this layer thickness depends on Ri_B and possibly on δ/H. Just below the critical level, Ri becomes much larger compared to its initial value due to the decreasing shear and the increasing stratification at this altitude. The shear reaches a maximum below the level of maximum acceleration ($\eta \approx 0.4H$) causing decaying Ri. The Richardson number, however, drops below zero at heights above $0.4H$. There, the shear decays and approaches zero. Therefore, we conclude that the mixing layer is mainly driven by the wave induced convective instability and not by a Kelvin–Helmholtz instability. In accordance with the flow picture of Fig. 2, the ocurrence of negative Ri at $t \approx 24H/\Delta U$ indicates the beginning of the breaking event.

The profiles of the perturbation kinetic energy $E = 0.5(\overline{u'^2} + \overline{v'^2} + \overline{w'^2})$, averaged over planes $\eta = \text{const}$, are shown in Fig. 5 for the DNS and LES at the same instances of time as in Fig. 4. Primed quantities denote deviations from the average. Hence, they contain both wavy and turbulent fluctuations. For the present discussion, a differentiation between wavy and turbulent fluctuations is not necessary, but will be subject of further studies. The kinetic energy E exhibits two maxima, one near the surface and one below the kinetic level. The first one is caused kinematically by the laminar flow over the wavy terrain. The second extreme value is produced dynamically by the breakdown of the vertically propagating internal gravity wave. It comprises contributions of the variances of u and w, whereas the variance of the cross-stream component v is roughly one order of magnitude smaller than $\overline{u'^2}$ (maximum value $\overline{v'^2}/\overline{u'^2} = 0.17$ for the LES and 0.09 for the DNS at $t = 40H/\Delta U$). Hence, the three-dimensionality is more pronounced in the LES

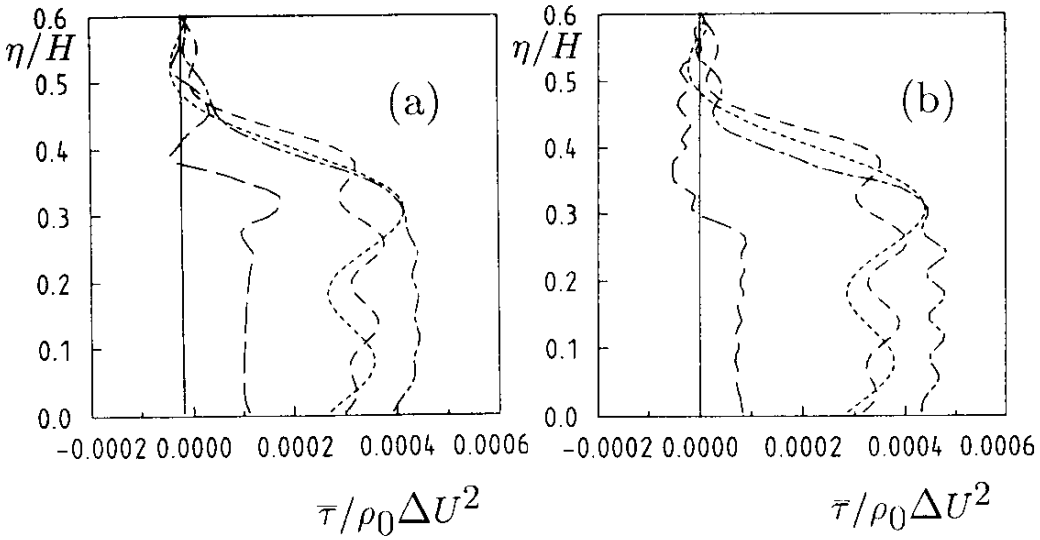

Fig. 6. Profiles of the momentum flux $\bar{\tau}$ for the DNS (a) and the LES (b). Line coding and averaging as in Fig. 4.

than in the DNS. Above the critical level, up to $0.6H$, the variances start to grow slightly in the early period but return to zero soon at later times. This illustrates the inhibition of the transmission of the approaching gravity waves through the forming critical layer.

Despite the two different breaking regimes, the total perturbation energy is nearly the same in the two cases. However, the energy evolves somewhat differently in the breaking area below the critical level: for $t > 20H/\Delta U$, E increases faster and then, after breaking, decreases slightly in the LES, whereas it grows continuously in the DNS owing to the sustained creation of secondary rolls. Obviously, the three-dimensional mixing in the LES is more effective and leads to a restratification of the fluid in the mixed layer which limits further mixing. Another remarkable result is the apparent sinking of the mixed layer due to entrainment at its lower edge. Sinking of thin turbulent layers has also been observed by radar in the free atmosphere [16].

One of the most important consequences of the absorption of a wave at the critical level is the acceleration of the mean flow (see Fig. 4). This acceleration requires a vertical gradient of the shear stress, because $\partial u/\partial t \sim -\partial\bar{\tau}/\partial z$, where τ is the vertical momentumm flux per unit volume. Idealized waves with infinite extent have a uniform momentum flux and the gradient is zero, i.e. on the average the fluid is never forced [5]. Figure 6 shows τ averaged over planes with constant coordinate η. Contributions to this flux are the resolved motions, the modelled fluxes of the frictional stresses, and an additional momentum flux due to pressure forces at the undulated surface (see [4]). In our simulations, the $\bar{\tau}$-profiles manifest a strong vertical structure (Fig. 6). Initially, the vertical flux of horizontal momentum is constant (zero for LES, slightly negative for DNS). At $t = 6H/\Delta U$, the $\bar{\tau}$-

profile exhibits vertically a wavelike structure. Its amplitude increases with altitude but strongly decreases to the initial value just below the critical level. Between $z \approx 0.3H$ and $z \approx 0.5H$, the gradient is negative and large and causes the strong acceleration of the mean flow. Due to the wavelike structure of the profiles, below this region other layers exist with an accelerated or decelerated motion. At $t > 12H/\Delta U$, the number of waves has been increased and at $t > 24H/\Delta U$, $\bar{\tau}$ is nearly uniform below the critical level. At late times after breaking, the shear stress is heavily reduced and becomes negative in the formerly forced region. The reduction is stronger in the LES than in the DNS, again indicating an enhanced turbulent mixing in the LES.

5. Conclusions

The nonlinear interaction of an internal gravity wave with its evolving critical level and the generation of a turbulently mixed layer has been investigated by means of DNS and LES, basically resembling flows with high and low viscosity. The flow structure in the DNS remains essentially laminar and becomes only weakly three-dimensional. The mixing takes place as a process of repeated rolling-up of isothermal (or density) surfaces so that the flow shows permanently overturning waves which generate vortical motions in a quasi periodic manner without real turbulence. Because of the weaker effective viscosity, the overturning waves in the LES break into three-dimensional turbulence resulting in faster mixing than in the DNS. In both cases, no Kelvin–Helmholtz instability is observed.

Further studies will be devoted to the characteristics of turbulence and their dependence on the effective Reynolds number of the flow. In addition we plan to compare our results to recently published findings of Andreassen et al. and Fritts et al. [1, 6], in particular with respect to the occurrence of organized lateral motions like streamwise vortices in the mixed region.

Acknowledgement

This work has been supported by the Deutsche Forschungsgemeinschaft.

References

1. Andreassen, Ø, Wasberg, C.E., Fritts, D.C. and Isler, J.R., Gravity breaking in two and three dimensions. 1. Model description and comparison of two-dimensional evolutions. *J. Geophys. Res.* 99 (1994) 8095–8108.
2. Booker, J.R. and Bretherton, F.P., The critical layer for internal gravity waves in a shear flow. *J. Fluid Mech.* 27 (1967) 513–539.
3. Delesi, D.P. and Dunkerton, T.J., Laboratory observations of gravity wave critical-layer flows. *Pure Appl. Geophys.* 130 (1989) 445–461.
4. Dörnbrack, A. and Schummann, U., Numerical simulation of turbulent convective flow over wavy terrain. *Bound. Layer Meteorol.* 65 (1993) 323–355.
5. Eliassen, A. and Palm, E., On the transfer of energy in stationary mountain waves. *Geofysiske Publikasjoner* XXXII (1960) 1–23.

6. Fritts, D.C., Isler, J.R. and Andreassen, Ø, Gravity breaking in two and three dimensions. 2. Three-dimensional evolution and instability structure. *J. Geophys. Res.* 99 (1994) 8109–8123.
7. Koop, C.G. and McGee, B., Measurements of internal gravity waves in a continuously stratified shear flow. *J. Fluid Mech.* 172 (1986) 453–480.
8. Kaltenbach, H.-J., Gerz, T. and Schumann, U., Large-eddy simulation of homogeneous turbulence and diffusion in stably stratified shear flow. *J. Fluid Mech.* 280 (1994) 1–40.
9. Krettenauer, K. and Schumann, U., Numerical simulation of turbulent convection over wavy terrain. *J. Fluid Mech.* 237 (1992) 261–299.
10. Lilly, D.K., On the numerical simulation of buoyant convection. *Tellus* 14 (1962) 148–172.
11. Nappo, C.J. and Chimonas, G., Wave exchange between the ground surface and a boundary-layer critical level. *J. Atmos. Sciences* 49 (1992) 1075–1091.
12. Nastrom, G.D. and Eaton, F.D., The coupling of gravity waves and turbulence at White Sands, New Mexico, from VHF radar observations. *J. Appl. Meteorol.* 32 (1993) 81–87.
13. Maaß, C. and Schumann, U., Numerical simulation of turbulent flow over a wavy boundary. In: Voke, P.R., Kleiser, L. and Chollet, J.P. (eds), *Direct and Large-Eddy Simulation I.* Dordrecht: Kluwer Academic Publishers (1994) pp. 287–297.
14. Merrill, J.T. and Grant J.R., A gravity wave – Critical level encounter observed in the atmospere. *J. Geophys. Res.* 84 (1979) 6315–6320.
15. Pao, Y. and Goldburg, A. (eds), *Clear Air Turbulence and Its Detection.* New York: Plenum Press (1969).
16. Sato, K. and Woodman, R.F., Fine altitude resolution radar observations of stratospheric layers by the Arecibo 430 MHz radar. *J. Atmos. Sciences* 39 (1982) 2546–2552.
17. Schumann, U., Hauf, T., Höller, H., Schmidt, H. and Volkert, H., A mesoscale model for the simulation of turbulence, clouds and flow over mountains: Formulation and validation examples. *Contr. Atmos. Phys., Beitr. Phys. Atmos.* 60 (1987) 413–446.
18. Sidi, C., Waves-turbulence coupling. In: Thrane, E.V. et al. (eds), *Coupling Processes in the Lower and Middle Atmosphere.* Dordrecht: Kluwer Academic Publishers (1993) pp. 291–304.
19. Smith, R.B., The influence of mountains on the atmosphere. *Adv. in Geophysics* 21 (1979) 87–230.
20. Thorpe, S.A., A method of producing a shear flow in a stratified fluid. *J. Fluid Mech.* 32 (1968) 693–704.
21. Thorpe, S.A., An experimental study of critical layers. *J. Fluid Mech.* 103 (1981) 321–344.